ACS APPLIED MATERIALS & INTERFACES

Research Article

www.acsami.org

DNA-Conjugated Quantum Dot Nanoprobe for High-Sensitivity Fluorescent Detection of DNA and micro-RNA

Shao Su,[†] Jinwei Fan,[†] Bing Xue,[†] Lihui Yuwen,*[,†] Xingfen Liu,[†] Dun Pan,[‡] Chunhai Fan,[†,‡] and Lianhui Wang*[,†]

[†]Key Laboratory for Organic Electronics & Information Displays (KLOEID), Institute of Advanced Materials (IAM), and School of Materials Science and Engineering, Nanjing University of Posts & Telecommunications, 9 Wenyuan Road, Nanjing 210046, China

[‡]Division of Physical Biology, Shanghai Institute of Applied Physics, Chinese Academy of Sciences, Shanghai 201800, China

Supporting Information

ABSTRACT: Herein, we report a convenient approach to developing quantum dots (QDs)-based nanosensors for DNA and micro-RNA (miRNA) detection. The DNA-QDs conjugate was prepared by a ligand-exchange method. Thiol-labeled ssDNA is directly attached to the QD surface, leading to highly water-dispersible nanoconjugates. The DNA-QDs conjugate has the advantages of the excellent optical properties of QDs and well-controlled recognition properties of DNA and can be used as a nanoprobe to construct a nanosensor for nucleic acid detection. With the addition of a target nucleic acid sequence, the fluorescence intensity of QDs was quenched by an organic quencher (BHQ_2) via Förster resonance energy transfer. This nanosensor can detect as low as 1 fM DNA and 10 fM miRNA. Moreover, the QDs-based nanosensor exhibited excellent selectivity. It not only can effectively distinguish single-base-mismatched and random nucleic sequences but also can recognize pre-miRNA and mature miRNA. Therefore, the nanosensor has high application potential for disease diagnosis and biological analysis.

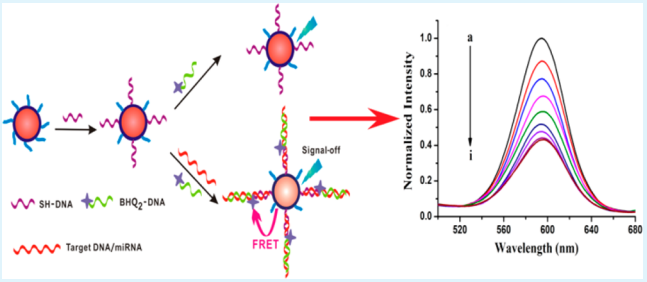

KEYWORDS: *quantum dots, DNA, micro-RNA, FRET, nanosensor*

INTRODUCTION

Nucleic acid detection (specifically, DNA and RNA analysis) is of high importance for clinical diagnosis, forensic analysis, and basic studies in the biological and biomedical fields.[1,2] In the past decades, simple, reliable, sensitive, and selective strategies for DNA detection have been developed by taking various sensing technologies such as fluorescence,[3,4] electric/electrochemical,[5−8] surface plasmon resonance,[9] surface-enhanced Raman scattering,[10,11] and so on. Nowadays, different strategies for highly sensitive and accurate micro-RNA (miRNA) detection have attracted the attention of the scientists. For example, specific miRNA may serve as biomarkers for the development of some cancers.[12] miRNAs are a group of small endogenous noncoding RNAs (approximately 18−25 nucleotides) that are well-known to play a critical role in hematopoietic differentiation, cell cycle, regulation, metabolism, tumor metastasis, stem-cell differentiation and renewal, and viral replication.[13] However, analysis of the intracellular levels of miRNAs is challenging because of their short lengths, low abundances, susceptibility to degradation, and sequence similarity among family members. Nowadays, several methods have been employed for miRNA analysis, including real-time quantitative polymerase chain reaction,[14] northern blotting,[15] electrochemical,[16,17] and miRNA array technology.[18] For example, Wen et al. reported a DNA nanostructure-based interfacial engineering approach to improve the miRNA detection sensitivity and selectivity.[16] Abell's group developed a simple and valid method for direct and label-free miRNA detection by surface-enhanced Raman spectroscopy technique.[11] Up to now, the development of simple, rapid and sensitive methods for the identification and quantification of miRNAs is still a challenge. Therefore, the development of versatile detection strategies for DNA and miRNA in vivo and in vitro has attracted the attention of more and more scientists.

For the last 2 decades, semiconductor quantum dots (QDs) were considered to be the ideal fluorescent markers in many fields, such as biosensing, biological imaging, immunoassay, and drug delivery because of their unique photophysical properties, such as size-tunable emission, broad absorption, narrow and symmetric photoluminescence (PL) spectra, high fluorescence quantum yields, and robust photostability. Alivisatos'[19] and Nie's[20] groups opened up an exciting QDs-based bionanotechnology field in 1998, which first used QDs in the biological field. Following their pioneering work, different QDs-based nanoprobes, which are constructed by conjugating protein, peptide, and DNA with QDs, have been employed in the

Received: October 30, 2013
Accepted: December 31, 2013
Published: December 31, 2013

   dx.doi.org/10.1021/am404811j | ACS Appl. Mater. Interfaces 2014, 6, 1152−1157

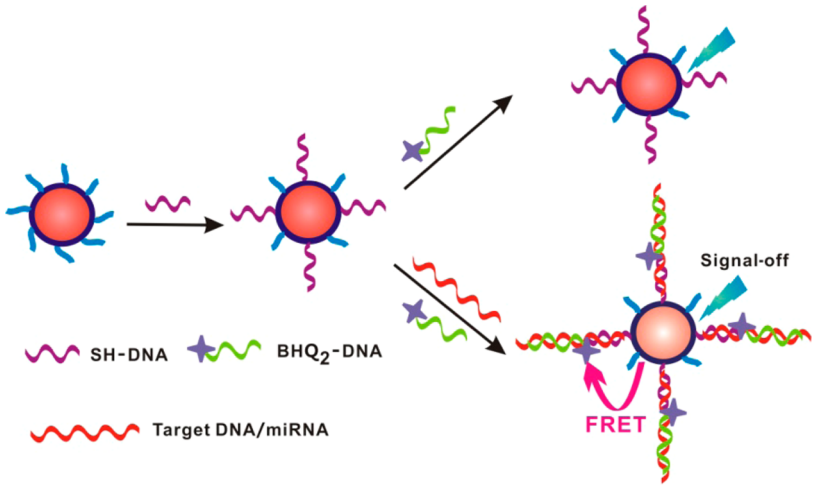

Figure 1. Schematic representation of the designed nanosensors for detection of DNA/miRNA based on the FRET system.

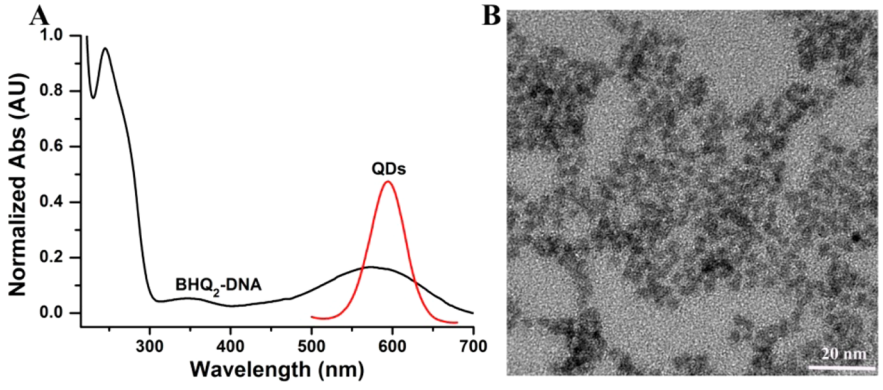

Figure 2. (A) Spectral overlap between QD emission and a BHQ_2-labeled DNA solution absorption. (B) Typical TEM image of MPA-capped QDs.

bionanotechnology field. As an example, three methods have been used to construct conjugated DNA-QDs, such as strepavidin-biotin,[21] EDC/NHS,[22] and ligand exchange.[23,24] Because of the drawbacks of functionalized techniques, the preparation of DNA-functionalized QDs for biological applications with high PL quantum yield and stability is still a challenge. In order to meet the requirements of biological applications, our group had also explored the method of biological molecule attachment to QDs. Compared with organic-phase QDs, aqueous-phase QDs possess excellent aqueous dispersibility and easily conjugate with DNA. Therefore, we have employed DNA-QDs (aqueous phase) conjugates as a bridge for carcinoembryonic antigen detection via ligand exchange.[25] Furthermore, we also developed a series of biomolecule-functionalized QDs for biomarker detection.[26,27]

In this work, we propose a versatile "signal-off" strategy for ultrahigh-sensitive and -selective DNA and miRNA detection. The CdTe/CdS core−shell QDs capped with 3-mercaptopropionic acid (MPA) were directly synthesized in the aqueous phase based on our previously reported microwave-assisted protocol.[28,29] Surface-bound short-chain MPA can be substituted by thiolated DNA via ligand exchange, leading to programmable DNA modification at the surface of QDs.[24] As shown in Figure 1, DNA-conjugated QDs were used as fluorescence nanoprobes for DNA and miRNA detection with strong PL and robust stability, in combination with the classic "sandwich" structure. In the absence of a target DNA/miRNA sequence, the organic quencher-labeled DNA has almost no influence on the DNA-QDs conjugate. With the addition of target DNA/miRNA and BHQ_2-labeled DNA sequences, sandwiched hybrids were formed. The fluorescence intensity of DNA-QDs has obviously decreased with the addition of a target DNA/miRNA sequence because of energy transfer from QDs to BHQ_2.

EXPERIMENTAL SECTION

Materials. DNA and miRNA oligonucleotides were synthesized and purified by Takara Biotechnology (Dalian, China). The sequences of these oligonucleotides are shown in the Supporting Information (Table S1). Tellurium powder (99.9%) and $CdCl_2$ (99.9%) were purchased from Aldrich. 3-Mercaptopropionic acid (MPA; 98%) was purchased from Fluka. $NaBH_4$ (99%) and Na_2S (99%) were obtained from Shanghai Chemical Reagents Company. All chemicals were used without additional purification. All solutions were prepared using Milli-Q water (Millipore) as the solvent.

Preparation of CdTe/CdS Core−Shell QDs. The monodispersed CdTe/CdS core−shell QDs capped with MPA were obtained via microwave irradiation, as described in our previous work.[28,29] Briefly, the CdTe precursor solution was prepared by adding a freshly prepared NaHTe solution to a N_2-saturated $CdCl_2$ solution in the presence of MPA as the stabilizer. CdTe QDs was prepared by heating the CdTe precursor solution at 100 °C for 1 min under microwave irradiation. The as-prepared CdTe solution was concentrated by rotatory evaporation and was then precipitated with 2-propanol followed by centrifugation at 12000 rpm. The CdTe/CdS precursor solution was prepared by adding the purified CdTe QDs water dispersion into an N_2-saturated CdS solution containing 2.1 μM CdTe QDs, 1.25 mM $CdCl_2$, 1.0 mM Na_2S, and 6.0 mM MPA at pH 8.4.

dx.doi.org/10.1021/am404811j | ACS Appl. Mater. Interfaces 2014, 6, 1152−1157

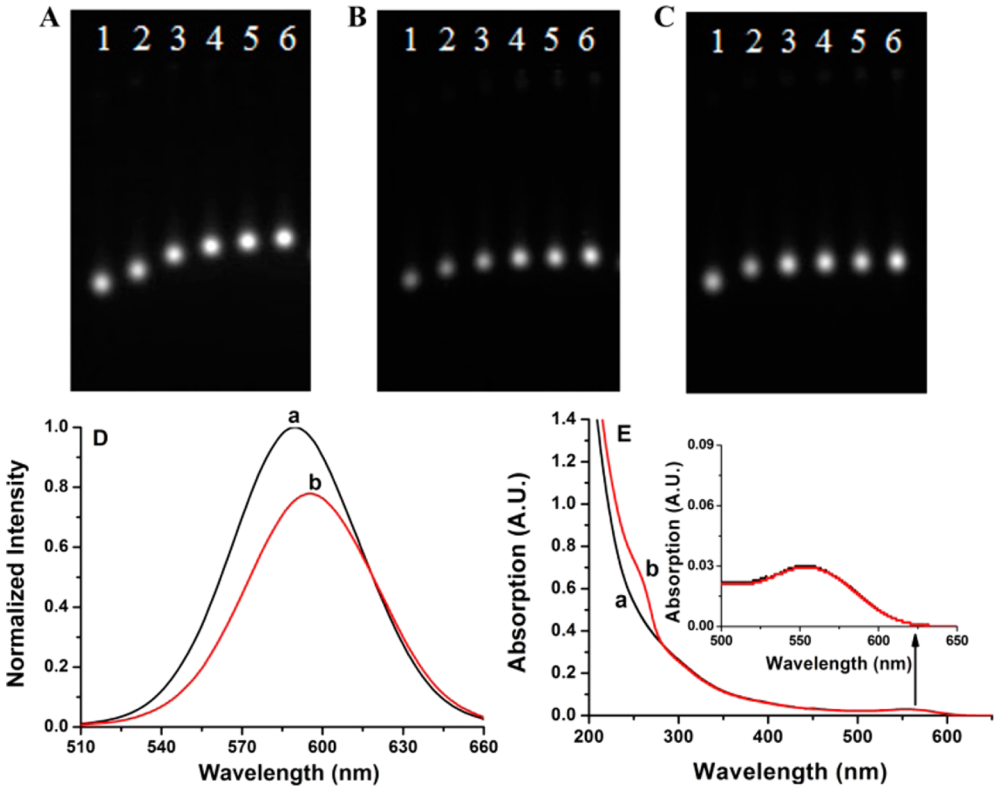

Figure 3. Agarose gel electrophoresis results of QDs at different conditions: (A) different molar ratios of QDs to SH-DNA (1 → 6: 1:0, 1:10, 1:20, 1:30, 1:40, and 1:50); (B) Different reaction times (1 → 6: 0, 12, 24, 36, 48, and 60 h); (C) Different reaction temperatures (1 → 6: only QDs, 20, 25, 30, 35, and 40 °C); (D) Fluorescence spectra of (a) MPA-QDs and (b) DNA-QDs; (E) UV−vis spectra of (a) MPA-QDs and (b) DNA-QDs.

The CdS shell was grown on the surface of the CdTe core in a quartz reaction tube with microwave irradiation at 120 °C for several minutes.

Modification of QDs with DNA. Thiolated DNA was directly attached to QDs via a ligand-exchange method. In order to obtain the DNA-conjugated QDs, the optimal experimental conditions have been investigated (such as the molar ratio of DNA to QDs, reaction time, and temperature). Briefly, some QDs were mixed with thiolated DNA at different temperatures for several hours in order to allow complete exchange of the MPA-capped QDs with the thiolated oligonucleotides. Then, the DNA-QDs conjugate was separated from the free oligonucleotides by ultrafiltration. After being centrifuged at 5500 rpm for 10 min, the supernatant was discarded and the pellet redispersed by 200 μL of Tris buffer. After three times, the obtained product was dissolved in a Tris-HCl buffer (10 mM, pH 7.6) to a desired concentration for measurement.

DNA/miRNA Hybridization. Hybridization experiments were performed in a 30 mM Tris-HCl buffer containing 0.1 M NaCl and 10 mM $MgCl_2$ at pH 7.6. The hybridization reaction was carried out by mixing 10 μL of the DNA-QDs conjugate (0.6 μM), 10 μL of the target DNA/miRNA sequence (2 μM), and 10 μL of BHQ_2-DNA (0.6 μM) at 37 °C for 30 min in a total volume of 200 μL. Control experiments without the addition of a target DNA/miRNA sequence were carried out simultaneously.

RESULTS AND DISCUSSION

UV−vis spectra of BHQ_2-labeled DNA (BHQ_2-DNA) and PL emission spectra of CdTe/CdS QDs are shown in Figure 2A. As can be seen, the maximum absorption peak of BHQ_2-DNA and the emission peak of QDs are 573 and 580 nm, respectively. The excellent spectral overlap between the absorption spectra of BHQ_2-DNA and the emission spectra of QDs can ensure efficient excited energy transfer from QDs to BHQ_2 based on the Förster resonance energy-transfer (FRET) mechanism.

As shown in Figure 2B, the transmission electron microscopy (TEM) image showed that the as-prepared CdTe/CdS QD was about 3 nm, which has nearly spherical morphology with good monodispersity. The fluorescent intensity was only decreased about 5% compared to the original QDs after 3 months, indicating that the obtained QDs showed high optical stability (see Figure S1 in the Supporting Information).

As is well-known, DNA attached on the surface of nanoparticles can change the gel electrophoresis velocity of the nanoparticles.[30] In order to verify the successful ligand exchange between MPA-QDs and SH-DNA, agarose gel electrophoresis has been employed to studied the samples of MPA-QDs and DNA-QDs .[31] A total of 10 μL of an as-prepared DNA-QDs conjugate solution under different conditions was loaded in 1% agarose gel in a dipotassium hydrogen phosphate solution (10 mM) and run at 50 V cm^{-1} to analyze their mobility (Figure 3A−C). As a control, 10 μL of a MPA-QDs solution was loaded in another lane. After electrophoresis for 90 min, the gel was illuminated by a UV lamp and the digital images were captured by a CCD. As shown in Figure 3, DNA-QDs run slower than MPA-QDs under the same conditions, which is ascribed to the larger size of the nanoprobe after the attachment of oligonucleotides to the surface of QDs. As can be seen from Figure 3A, increasing the molar ratio of DNA-QDs will decrease the mobility of DNA-QDs, while at relative higher DNA-QDs ratios (1:40 and 1:50), the mobility of the DNA-QDs conjugate reached a plateau, which indicates that the attachment of DNA to the surface of QDs nearly saturates. Therefore, we choose 30:1 as the optimal DNA-QDs molar ratio in this work. Moreover, the reaction temperature and reaction time were also carefully studied. In this work, the optimum reaction temperature and reaction time

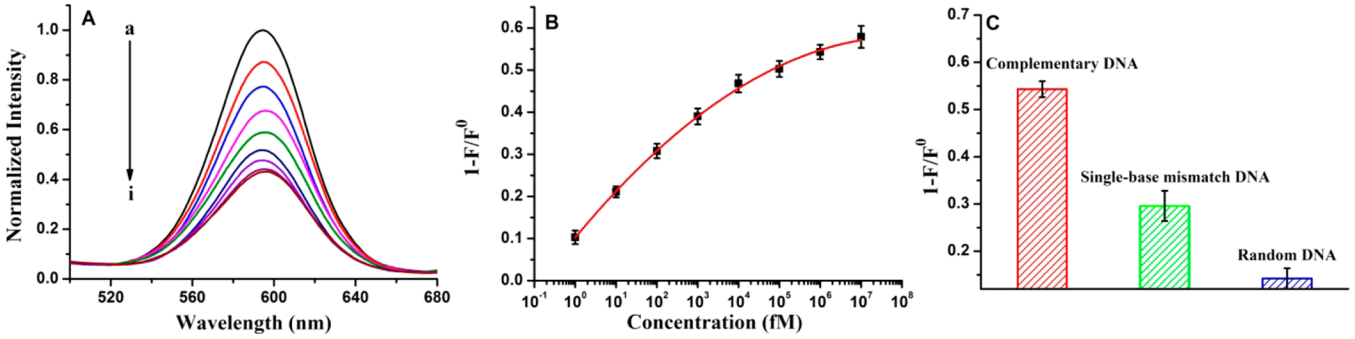

Figure 4. (A) Emission spectra of nanosensor containing different concentrations of target DNA (a → i: 0, 1 fM, 10 fM, 100 fM, 1 pM, 10 pM, 100 pM, 1 nM, and 10 nM). (B) Dose-response calibration curve for target DNA based on the nanosensor. (C) Quenching efficiency of complementary target, single-base-mismatched, and random DNA.

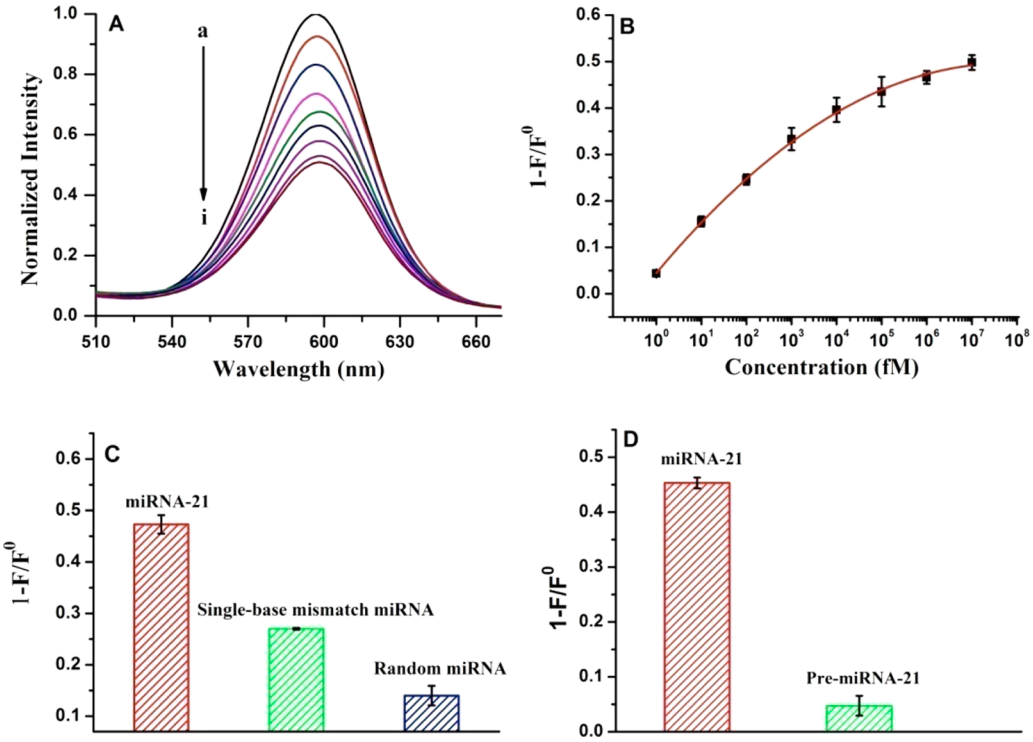

Figure 5. (A) Emission spectra of nanosensors containing different concentrations of miRNA-21 (a → i: 0, 1 fM, 10 fM, 100 fM, 1 pM, 10 pM, 100 pM, 1 nM, and 10 nM). (B) Dependence of the quenching rate and concentration of miRNA-21 based on the nanosensor. (C) Quenching efficiency of complementary, single-base-mismatched, and random miRNA. (D) Quenching efficiency of pre-miRNA-21 and miRNA-21.

were chosen as 25 °C (Figure 3B) and 36 h (Figure 3C), respectively.

Under the optimum conditions, the fluorescence intensity of DNA-QDs conjugates is little lower than that of the pure QDs and the shape of the emission peak is almost the same before and after the modification of QDs with SH-DNA, suggesting DNA-QDs exhibited excellent stability of covalent conjugation between QDs and SH-DNA. Moreover, the maximum emission wavelength showed a slight red shift from 585 to 595 nm, which was ascribed to the increase of QDs' size (Figure 3D). As is well-known, the number of the DNA attached on the surface of QDs directly affects the efficiency of DNA hybridization and the detection limit of the target DNA. Therefore, UV−vis spectroscopy was used to evaluate the efficiency of the ligand exchange between MPA capped on QDs and SH-DNA. As shown in Figure 3E, the absorption spectra of DNA and QDs were 260 and 555 nm, respectively. On the basis of the equations,[32] DNA and QDs were calculated to be 1.58 and 0.34 nM, indicating that the molar ratio of DNA-QDs was about 5:1. In other words, five SH-DNAs were attached to one QD surface via ligand exchange.

The DNA-QDs conjugate was used as a nanoprobe for target DNA detection through hybridization reaction to form a classic "sandwich" structure in the presence of target DNA and BHQ_2-labeled DNA (Figure 1). The fluorescence intensity of QDs was only decreased 3.2% compared to the original DNA-QDs conjugate in the absence of complementary target DNA, indicating that the noncomplementary BHQ_2-DNA had almost no influence on DNA-QDs (see Fig. S2 in the Supporting Information). While the target DNA was added, the fluorescence intensity of 30 nM DNA-QDs obviously decreased because the excited energy was transferred from QDs to the quencher (BHQ_2). As shown in Figure 4A, the fluorescence intensity of QDs decreased proportionally to the target DNA

dx.doi.org/10.1021/am404811j | ACS Appl. Mater. Interfaces 2014, 6, 1152−1157

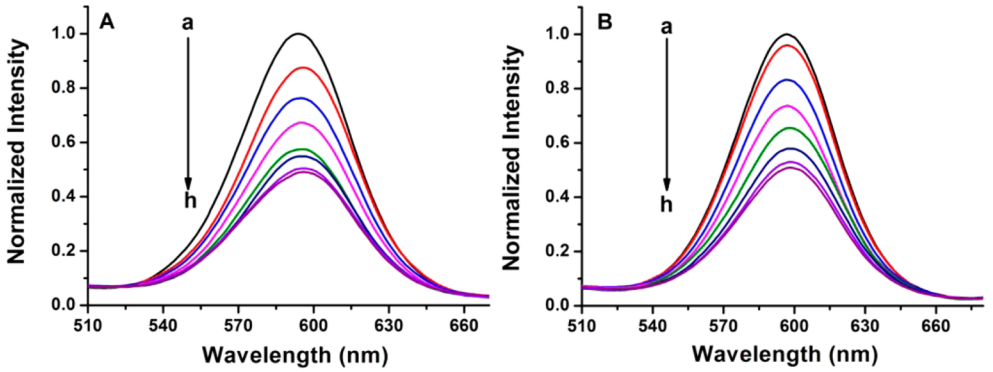

Figure 6. (A) Emission spectra of nanosensor containing different concentrations of target DNA in the serum (a → h: 0, 10 fM, 100 fM, 1 pM, 10 pM, 100 pM, 1 nM, and 10 nM). (B) Emission spectra of nanosensor containing different concentrations of target miRNA-21 in the serum (a → h: 0, 10, and 100 fM, 1, 10, and 100 pM, and 1 and 10 nM).

concentration in the range from 1 fM to 10 nM. The fluorescence intensity of QDs decreased monotonically with the logarithm concentration of target DNA, resulting in a typical dose−response curve (Figure 4B). Because the fluorescence intensity of QDs decreased 8%, which is larger than that when no target DNA was added, the nanosensor can detect as low as 1 fM DNA. Furthermore, the selectivity of the QDs-based nanosensor was studied. As shown in Figure 4C, the fluorescence intensity of QDs decreased 54.3%, 29.6%, and 14.2% in the presence of target, single-base-mismatched, and random DNA with the same concentration (1 nM), respectively, suggesting that the nanosensor can obviously distinguish the single-base-mismatched and random DNA.

On the basis of the above results, the QDs-based nanosensor was also used to detect miRNA-21. As expected, the QDs-based nanosensor displayed excellent performance for miRNA-21 detection. Obviously, the fluorescence intensity of QDs decreased with miRNA-21 addition (Figure 5A). When the concentration of miRNA-21 was 10 nM, the decreased fluorescence intensity of QDs reached a plateau. We challenged the QDs-based nanosensor with a series of concentrations of the synthetic miRNA-21 in the range from 1 fM to 10 nM. As shown in Figure 5B, the fluorescence intensity of QDs was decreased monotonically with the logarithm concentration of miRNA-21, which is similar to the DNA detection sensitivity achieved with the nanosensor. The detection limit of the nanosensor was determined to be 10 fM, which is higher than the detection limit of DNA detection by the same nanosensor.

The specificity of the QDs-based nanosensor was also investigated. Significantly, the nanosensor can effectively differentiate miRNA-21 and single-base-mismatched and random RNA (Figure 5C). Moreover, the QDs-based nanosensor can also effectively differentiate precursor miRNAs (pre-miRNAs) from mature ones. Pre-miRNAs are spliced in vivo to form mature miRNAs, which are then assembled into active RNA-induced silencing complexes. Their coexistence often results in false positives in medical assays. We then challenged the nanosensor with a hairpin-structured precursor human miRNA (pre-miRNA-21) and synthetic miRNA-21 sequences. As shown in Figure 5D, the fluorescence quenching rate of the synthetic miRNA-21 was nearly 10 times than that for pre-miRNA-21, suggesting that the QDs-based nanosensor can suppress the signal for pre-miRNAs and realize error-free detection of miRNAs.

To test the feasibility of the practical application of the QDs-based sensor, we conducted analyses of DNA and miRNA-21 in bovine serum. Different concentrations of DNA (Figure 6A) or miRNA-21 (Figure 6B) were added to the diluted (50-fold) serum samples. With the target DNA or miRNA-21 addition, the fluorescent intensity was decreased. The calibration curve in the presence of 2% serum was similar to that in the Tris-HCl buffer. The fluorescence intensity of QDs decreased proportionally to the target DNA and miRNA concentrations in the ranges from 10 fM to 10 nM and from 100 fM to 10 nM, respectively. The QDs-based nanosensor can detect target DNA and miRNA-21 as low as 10 and 100 fM in 2% serum, respectively.

CONCLUSIONS

In summary, we used the DNA-QDs conjugate as a fluorescence nanoprobe to detect DNA/miRNA based on the FRET process. The DNA-QDs conjugate was prepared by a ligand-exchange method, which possesses the high fluorescence property of QDs and recognition of DNA. This nanosensor exhibited excellent sensitivity, selectivity, and repeatability, which have application potential in biological analysis and clinical diagnosis.

ASSOCIATED CONTENT

Supporting Information

Sequences of these oligonucleotides (Table S1), storage stability of QDs (Figure S1), and PL spectra of DNA-QDs and DNA-QDs mixed with BHQ_2-DNA (Figure S2). This material is available free of charge via the Internet at http://pubs.acs.org.

AUTHOR INFORMATION

Corresponding Authors

*E-mail: iamlhyuwen@njupt.edu.cn. Tel: +86 25 85866333.
*E-mail: iamlhwang@njupt.edu.cn. Tel: +86 25 85866333.

Notes

The authors declare no competing financial interest.

ACKNOWLEDGMENTS

This work was financially supported by the National Basic Research Program of China (Grants 2012CB933301 and 2009CB930600), the National Natural Science Foundation of China (Grants 21305070, 21204038, 81273409, and 21375139), the Ministry of Education of China (Grants IRT1148 and 20123223110007), the Priority Academic Program Development of Jiangsu Higher Education Institu-

tions, the Open Research Fund of State Key Laboratory of Bioelectronics (Southeast University), and the Open Research Fund of State Key Laboratory of Coordination Chemistry (Nanjing University).

REFERENCES

(1) Sidransky, D. *Science* **1997**, *278*, 1054−1058.
(2) Hill, H. D.; Mirkin, C. A. *Nat. Protoc.* **2006**, *1*, 324−336.
(3) Smith, L. M.; Sanders, J. Z.; Kaiser, R. J.; Hughes, P.; Dodd, C.; Connell, C. R.; Heiner, C.; Kent, S. B.; Hood, L. E. *Nature* **1986**, *321*, 674−679.
(4) He, S.; Song, B.; Li, D.; Zhu, C.; Qi, W.; Wen, Y.; Wang, L.; Song, S.; Fang, H.; Fan, C. *Adv. Funct. Mater.* **2010**, *20*, 453−459.
(5) Fan, C.; Plaxco, K. W.; Heeger, A. J. *Proc. Natl. Acad. Sci. U.S.A.* **2003**, *100*, 9134−9137.
(6) Wu, S.; He, Q.; Tan, C.; Wang, Y.; Zhang, H. *Small* **2013**, *9*, 1160−1172.
(7) Wang, Z.; Zhang, J.; Yin, Z.; Wu, S.; Mandler, D.; Zhang, H. *Nanoscale* **2012**, *4*, 2728−2733.
(8) Wang, Z.; Zhang, J.; Chen, P.; Zhou, X.; Yang, Y.; Wu, S.; Niu, L.; Han, Y.; Wang, L.; Boey, F. *Biosens. Bioelectron.* **2011**, *26*, 3881−3886.
(9) Goodrich, T. T.; Lee, H. J.; Corn, R. M. *J. Am. Chem. Soc.* **2004**, *126*, 4086−4087.
(10) Cao, Y. C.; Jin, R.; Mirkin, C. A. *Science* **2002**, *297*, 1536−1540.
(11) Abell, J. L.; Garren, J. M.; Driskell, J. D.; Tripp, R. A.; Zhao, Y. *J. Am. Chem. Soc.* **2012**, *134*, 12889−12892.
(12) Calin, G. A.; Croce, C. M. *Nat. Rev. Cancer* **2006**, *6*, 857−866.
(13) Bartel, D. P. *Cell* **2004**, *116*, 281−297.
(14) Design, R.-T. P. P. *Biotechniques* **2005**, *39*, 519−525.
(15) Várallyay, É.; Burgyán, J.; Havelda, Z. *Nat. Protoc.* **2008**, *3*, 190−196.
(16) Wen, Y.; Pei, H.; Shen, Y.; Xi, J.; Lin, M.; Lu, N.; Shen, X.; Li, J.; Fan, C. *Sci. Rep.* **2012**, *2*, 867.
(17) Yin, H.; Zhou, Y.; Zhang, H.; Meng, X.; Ai, S. *Biosens. Bioelectron.* **2012**, *33*, 247−253.
(18) Lim, L. P.; Lau, N. C.; Garrett-Engele, P.; Grimson, A.; Schelter, J. M.; Castle, J.; Bartel, D. P.; Linsley, P. S.; Johnson, J. M. *Nature* **2005**, *433*, 769−773.
(19) Bruchez, M.; Moronne, M.; Gin, P.; Weiss, S.; Alivisatos, A. P. *Science* **1998**, *281*, 2013−2016.
(20) Chan, W. C.; Nie, S. *Science* **1998**, *281*, 2016−2018.
(21) Sharma, J.; Ke, Y.; Lin, C.; Chhabra, R.; Wang, Q.; Nangreave, J.; Liu, Y.; Yan, H. *Angew. Chem., Int. Ed.* **2008**, *47*, 5157−5159.
(22) Zhou, D.; Ying, L.; Hong, X.; Hall, E. A.; Abell, C.; Klenerman, D. *Langmuir* **2008**, *24*, 1659−1664.
(23) Zhou, D.; Piper, J. D.; Abell, C.; Klenerman, D.; Kang, D.-J.; Ying, L. *Chem. Commun.* **2005**, *38*, 4807−4809.
(24) Mitchell, G. P.; Mirkin, C. A.; Letsinger, R. L. *J. Am. Chem. Soc.* **1999**, *121*, 8122−8123.
(25) Hu, M.; He, Y.; Song, S.; Yan, J.; Lu, H.-T.; Weng, L.-X.; Wang, L.-H.; Fan, C. *Chem. Commun.* **2010**, *46*, 6126−6128.
(26) Yan, J.; Hu, M.; Li, D.; He, Y.; Zhao, R.; Jiang, X.; Song, S.; Wang, L.; Fan, C. *Nano Res.* **2008**, *1*, 490−496.
(27) Hu, M.; Yan, J.; He, Y.; Lu, H.; Weng, L.; Song, S.; Fan, C.; Wang, L. *ACS Nano* **2009**, *4*, 488−494.
(28) He, Y.; Lu, H.-T.; Sai, L.-M.; Lai, W.-Y.; Fan, Q.-L.; Wang, L.-H.; Huang, W. *J. Phys. Chem. B* **2006**, *110*, 13370−13374.
(29) He, Y.; Lu, H. T.; Sai, L. M.; Su, Y. Y.; Hu, M.; Fan, C. H.; Huang, W.; Wang, L. H. *Adv. Mater.* **2008**, *20*, 3416−3421.
(30) Parak, W. J.; Gerion, D.; Zanchet, D.; Woerz, A. S.; Pellegrino, T.; Micheel, C.; Williams, S. C.; Seitz, M.; Bruehl, R. E.; Bryant, Z. *Chem. Mater.* **2002**, *14*, 2113−2119.
(31) Medintz, I. L.; Berti, L.; Pons, T.; Grimes, A. F.; English, D. S.; Alessandrini, A.; Facci, P.; Mattoussi, H. *Nano Lett.* **2007**, *7*, 1741−1748.
(32) Yu, W. W.; Qu, L.; Guo, W.; Peng, X. *Chem. Mater.* **2003**, *15*, 2854−2860.